



LAWRENCE  
LIVERMORE  
NATIONAL  
LABORATORY

# Near-field nanoimaging of colloidal transition metal dichalcogenide waveguides

J. Li, R. Yang, K. Yao, Y. Huang, Y. Rho, D. E. Fan, Y. Zhang, C. P. Grigoropoulos

October 31, 2023

Advanced Functional Materials

## **Disclaimer**

---

This document was prepared as an account of work sponsored by an agency of the United States government. Neither the United States government nor Lawrence Livermore National Security, LLC, nor any of their employees makes any warranty, expressed or implied, or assumes any legal liability or responsibility for the accuracy, completeness, or usefulness of any information, apparatus, product, or process disclosed, or represents that its use would not infringe privately owned rights. Reference herein to any specific commercial product, process, or service by trade name, trademark, manufacturer, or otherwise does not necessarily constitute or imply its endorsement, recommendation, or favoring by the United States government or Lawrence Livermore National Security, LLC. The views and opinions of authors expressed herein do not necessarily state or reflect those of the United States government or Lawrence Livermore National Security, LLC, and shall not be used for advertising or product endorsement purposes.

## **Near-field nanoimaging of colloidal transition metal dichalcogenide waveguides**

*Jingang Li, Rundi Yang, Kan Yao, Yun Huang, Yoonsoo Rho, Donglei Emma Fan, Yuebing Zheng, Costas P. Grigoropoulos\**

Dr. J. Li, R. Yang, Dr. Y. Rho, Prof. C. P. Grigoropoulos

Laser Thermal Laboratory, Department of Mechanical Engineering, University of California, Berkeley, CA 94720, USA.

Email: [cgrigoro@berkeley.edu](mailto:cgrigoro@berkeley.edu)

Dr. K. Yao, Dr. Y. Huang, Prof. D. E. Fan, Prof. Y. Zheng

Walker Department of Mechanical Engineering, Materials Science & Engineering Program and Texas Materials Institute, University of Texas at Austin, Austin, TX 78712, USA.

Dr. Y. Rho

Physical & Life Sciences and NIF & Photon Sciences, Lawrence Livermore National Laboratory, Livermore, CA 94550, USA.

Keywords: colloidal nanowires, near-field imaging, transition metal dichalcogenides, waveguides

## **Abstract**

Bulk transition metal dichalcogenide (TMDC) nanostructures have been regarded as promising material candidates for integrated photonics due to their high refractive index at the near-infrared wavelengths. In this work, colloidal TMDC waveguides with tailorable dimensions are prepared by a scalable synthetic approach. The optical waveguiding properties of colloidal nanowires are studied by the near-field nanoimaging technique. In addition to dependence on thickness and wavelength, the excitonic responses and resultant waveguide modes in TMDC nanowires can be modulated by the environmental temperature. With the high-throughput production and tunable optical properties, colloidal TMDC nanowires highlight the potential for active optical components and integrated photonic devices.

## **Main text**

The emerging transition metal dichalcogenides (TMDCs) have demonstrated remarkable physical properties, including tunable bandgaps, strong photoluminescence from monolayers, strong excitonic effects, and valley polarization.<sup>[1-4]</sup> They have been widely exploited for many optoelectronic applications, including photodetection and light emission,<sup>[5, 6]</sup> with the potential to outperform conventional semiconductor materials.

While monolayer and few-layer TMDCs continue attracting intensive research attention, bulk TMDCs are recently realized to be promising dielectric materials with high refractive indexes, which highlight notable advantages in low optical loss and high compatibility with the prevailing silicon electronics.<sup>[7]</sup> High-index dielectric nanostructures also support strong electric and magnetic Mie resonances that are suitable for optical nanoantennas and metasurfaces.<sup>[8]</sup> Silicon-based metamaterials have been extensively investigated for wavefront control, chiral optics, topological nanophotonics, and nonlinear optics, etc.<sup>[9-12]</sup> Recently, TMDC nanostructures have been studied as dielectric nanoresonators to simultaneously support pronounced Mie and excitonic resonances.<sup>[13-15]</sup> The strong coupling between intrinsic excitons and geometrical resonances leads to tunable exciton polaritons in TMDC nanostructures,<sup>[13, 16, 17]</sup> providing a simple and compact materials platform for active polaritonic and optoelectronic devices.

In addition, TMDCs feature higher refractive indexes in the visible and near-infrared regimes than those of silicon and common III-V semiconductors (Figure S1, Supporting Information),<sup>[18, 19]</sup> which is favorable for a variety of integrated photonic applications. Optical components made of bulk TMDCs are predicted to have superior performances compared with conventional semiconductors.<sup>[20]</sup> Experimental demonstrations of subwavelength TMDC nanostructures for light confinement and waveguiding have also

been reported.<sup>[21, 22]</sup> However, current methods to prepare TMDC nanostructures rely on advanced lithographical strategies, which usually involve complex steps and careful testing procedures.<sup>[22]</sup> In this regard, a versatile and high-throughput approach to produce TMDC nanostructures is highly desired to fully unleash their potential for practical nanophotonics. Here, we show the chemically synthesized high-quality TMDC nanowires can function as optical waveguides with tailorable dimensions and optical responses. We present the near-field study of colloidal MoS<sub>2</sub> waveguides (**Figure 1a**) and investigate the dispersion relations with variable thicknesses and incident laser wavelengths. The temperature-dependent excitonic properties of MoS<sub>2</sub> also result in tunable optical waveguiding properties, which offers additional flexibility in designing active integrated photonic devices.

MoS<sub>2</sub> nanowires are synthesized via a two-step sulfurization reaction (see Experimental Section and Figure S2).<sup>[23]</sup> MoO<sub>3</sub> nanowires function as both the precursor material and the template to control the size of final MoS<sub>2</sub> nanowires. The as-synthesized colloidal nanowires with tunable dimensions can be easily deposited onto any substrates (Figure 1b). Figure 1c shows the typical scanning electron microscopy (SEM) images of the MoS<sub>2</sub> nanowires with a length of 5-20 μm. The composition and chemical purity of the final product is confirmed with Raman spectroscopy (Figure 1d), where the representative E<sub>2g</sub><sup>1</sup> and A<sub>1g</sub> bands can be identified.<sup>[24]</sup>

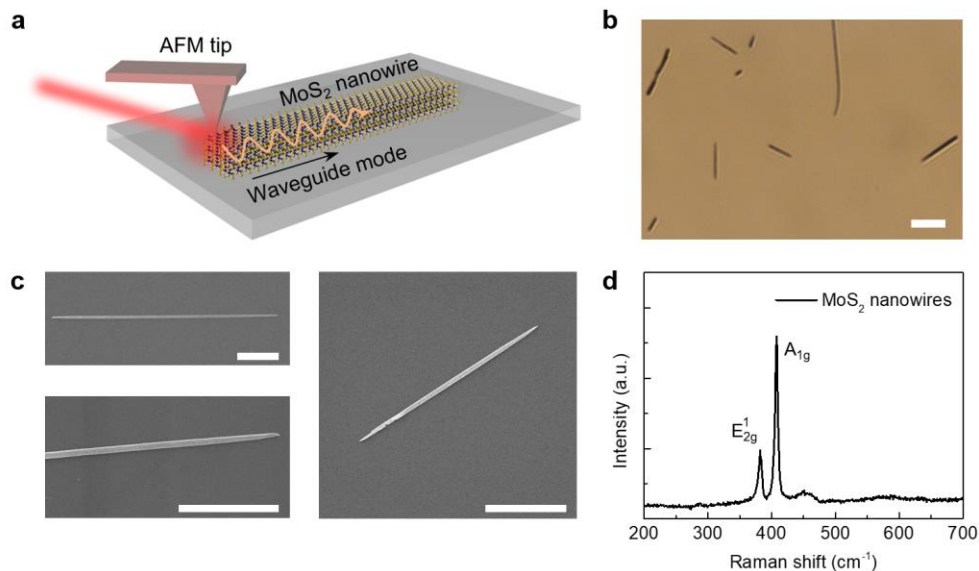


**Figure 1.** General concept and characterizations of colloidal MoS<sub>2</sub> nanowires. a) Schematic showing the near-field imaging of MoS<sub>2</sub> waveguides. b) Optical images of the deposited colloidal MoS<sub>2</sub> nanowires with varying dimensions. c) SEM images of colloidal MoS<sub>2</sub> nanowires. d) Raman spectrum of MoS<sub>2</sub> nanowires. Scale bars: (b) 10 μm, (c) 5 μm.

The optical waveguiding properties of individual colloidal MoS<sub>2</sub> nanowires are investigated by the near-field nanoimaging technique, known as scattering-type scanning near-field optical microscopy (s-SNOM, see Experimental Section).<sup>[25, 26]</sup> Compared with far-field methods, such nanoimaging technique enables the direct visualization of real-space distribution and propagation of localized electromagnetic fields within the subwavelength waveguides.<sup>[27-29]</sup> **Figure 2a-c** show three colloidal MoS<sub>2</sub> waveguides with the thickness of 60, 80, and 95 nm, respectively. The corresponding near-field images are presented in Figure 2d-f, where clear fringe patterns along the nanowire axis can be observed. During the near-field measurement, the incident laser beam with a wavelength of 800 nm is directed onto an atomic force microscope (AFM) tip to excite the waveguide modes, which propagate along the MoS<sub>2</sub> nanowire and get scattered at the sample edge. The fringe patterns are generated by the interference between the tip-scattered light and edge-scattered photons (Figure S3). The in-plane wavevector  $q$ , i.e., the propagation constant, of the excited waveguide mode in a MoS<sub>2</sub> nanowire can be determined by the fringe period  $\rho$  by<sup>[27]</sup>

$$\frac{q}{k_0} = \frac{\lambda_0}{\rho} + \cos\theta\cos\alpha \quad (1)$$

where  $\lambda_0$  and  $k_0$  are the wavelength and wavevector of the incident light, respectively.  $\theta$  is the incident angle, and  $\alpha$  is the angle between the nanowire axis and the projection of incident light in the sample plane (see Figure S3 for the detailed configurations).

To accurately extract the fringe period  $\rho$  for wavevector analysis, we plot the real-space amplitude of the fringe profiles (Figure 2g) and apply Fourier transform (FT) to obtain information in the momentum space. The FT profiles show two distinct peaks, including the low-frequency air mode<sup>[28]</sup> and the waveguide mode  $E_{11}^x$ . The wavevector of the air mode remains largely unchanged with the varying thickness. In contrast, the wavevector of the  $E_{11}^x$  mode clearly shifts to higher frequencies for thicker MoS<sub>2</sub> nanowires (Figure 2h). The in-plane wavevectors are then calculated based on Equation 1 and plotted in Figure 2i. According to Marcatili method for the rectangular dielectric waveguide model,<sup>[30]</sup> the wavevector  $q$  of  $E_{mn}^x$  mode can be written as

$$q = \sqrt{\varepsilon k_0^2 - (k_x^2 + k_y^2)} \quad (2)$$

with

$$\tan(k_x d) = \frac{k_x \left( \sqrt{(\varepsilon - \varepsilon_s)k_0^2 - k_x^2} + \sqrt{(\varepsilon - \varepsilon_a)k_0^2 - k_x^2} \right)}{k_x^2 - \sqrt{(\varepsilon - \varepsilon_s)k_0^2 - k_x^2} \sqrt{(\varepsilon - \varepsilon_a)k_0^2 - k_x^2}} \quad (3)$$

$$\tan(k_y w) = \frac{2k_y \varepsilon \varepsilon_a \sqrt{(\varepsilon - \varepsilon_a)k_0^2 - k_y^2}}{\varepsilon_a^2 k_y^2 - \varepsilon^2 [(\varepsilon - \varepsilon_a)k_0^2 - k_y^2]} \quad (4)$$

where  $k_x$  and  $k_y$  are transverse wavevector components in the cross-sectional plane,  $\epsilon$ ,  $\epsilon_a$ , and  $\epsilon_s$  are the relative dielectric constants of MoS<sub>2</sub>, air, and the substrate, respectively,  $d$  and  $w$  are thickness and width of the nanowire, respectively (see Inset in Figure 2i);  $m$  and  $n$  stand for different mode numbers and are obtained from the solutions of Eqs. (3) and (4). We calculate the theoretical wavevectors of the  $E_{11}^x$  mode as a function of waveguide thickness, which agree well with the experimental results (Figure 2i). The simulated mode profiles are also shown in Figure S4, where the high-index MoS<sub>2</sub> nanowires can confine electric fields in the waveguide with minimal leakage.

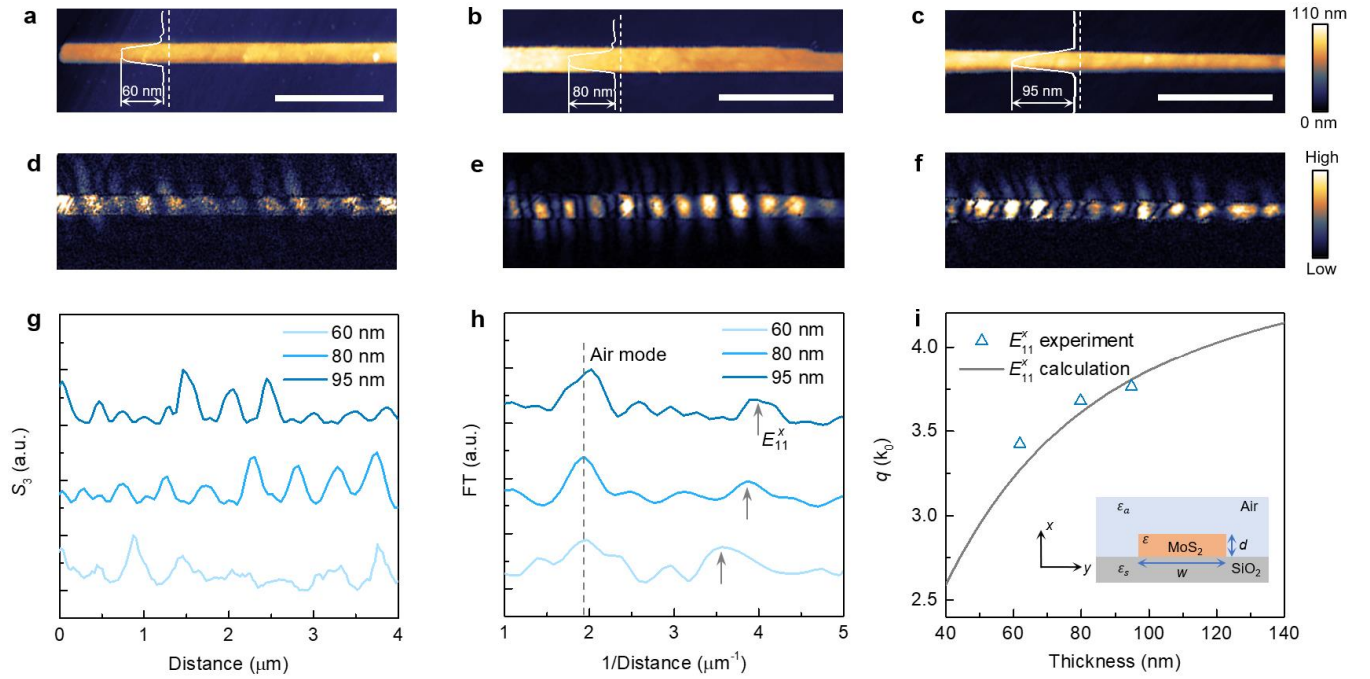


**Figure 2.** Near-field imaging of MoS<sub>2</sub> nanowires with different thicknesses. a-c) AFM images of three MoS<sub>2</sub> nanowires with the thickness of (a) 60 nm, (b) 80 nm, and (c) 95 nm. The height profiles across the nanowire axis are embedded. d-f) The corresponding near-field images of MoS<sub>2</sub> nanowires in (a-c). The incident wavelength is 800 nm. g,h) Real-space fringe profiles and corresponding FT profiles extracted from (d-f). i) Experimental and theoretical thickness dispersions of the  $E_{11}^x$  waveguide mode. Insets show the cross-sectional view of the waveguide configuration. Scale bars: (a-c) 2  $\mu\text{m}$ .

To determine the propagation length ( $L_p$ ) of the waveguide mode, we perform an inverse Fourier transform process for the FT profile after filtering out the short ( $< 3 \mu\text{m}^{-1}$ ) and long ( $> 5 \mu\text{m}^{-1}$ ) spatial frequencies.<sup>[29]</sup> The fitting of this new fringe profile with an exponentially decaying envelope yields a propagation length  $L_p \approx 3.1 \mu\text{m}$  (Figure S5). The obtained propagation length is similar to that of reported

TMDC waveguides prepared from exfoliated flakes,<sup>[27, 29]</sup> indicating the high materials quality of our colloidal nanowires.

Next, we study the dispersion of the MoS<sub>2</sub> waveguide. **Figure 3a** shows near-field images of the same nanowire in Figure 2c at different excitation wavelengths ( $\lambda_0$ ). The real-space fringe amplitude and the corresponding FT profiles are presented in Figure 3b and Figure 3c, respectively. With increasing wavelengths, the  $E_{11}^x$  mode moves toward lower frequencies. We calculate the theoretical wavelength-dependent wavevectors of the  $E_{11}^x$  mode based on Equation 2, and the results match with the experimentally obtained in-plane wavevectors (Figure 3d).

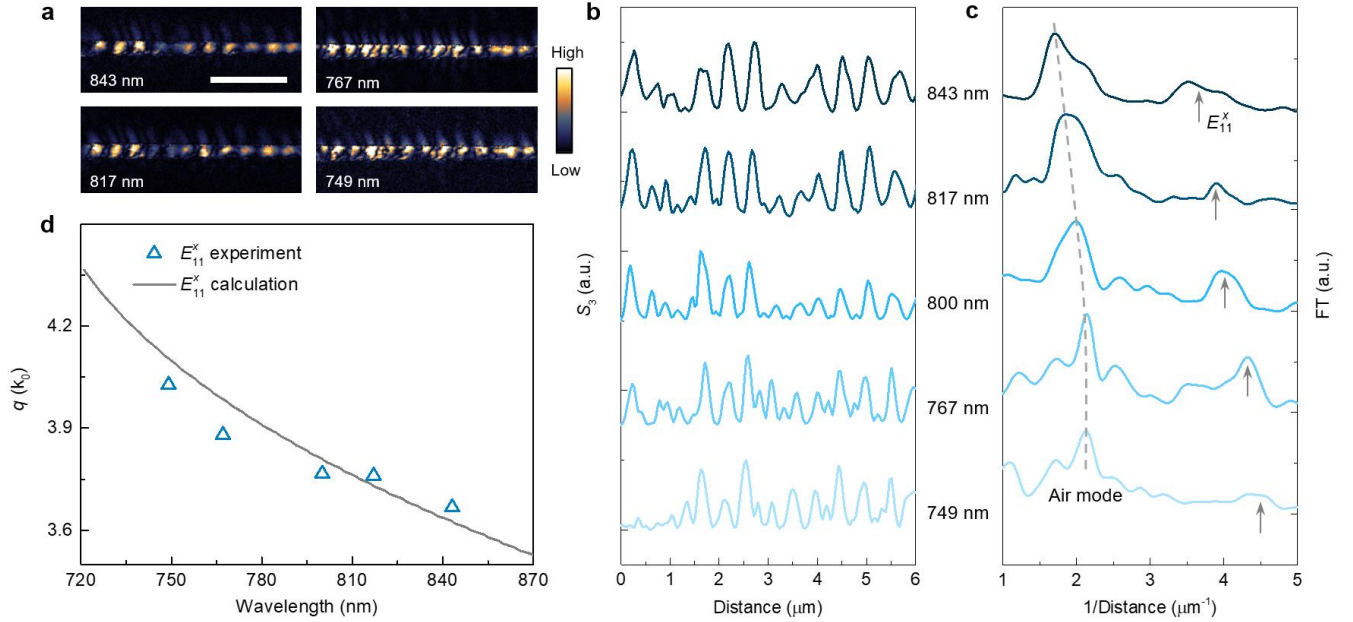


**Figure 3.** Wavelength dependence study. a) Near-field images of a MoS<sub>2</sub> nanowire with a thickness of 95 nm under different laser wavelengths. b,c) The real-space fringe profiles and corresponding FT profiles. d) Experimental and theoretical data of the  $E_{11}^x$  mode. Scale bar: (a) 2 μm.

Last, we explore the possibility of modulating optical waveguiding properties by changing the environmental temperature. With a customized heating stage in the experimental setup, we measure the temperature-dependent near-field images of a MoS<sub>2</sub> nanowire (**Figure 4a**). By tracking the peaks in the FT profiles of the fringes (Figure 4b), we observe the increasing spatial frequencies of the  $E_{11}^x$  mode under the elevated temperature (Figure 4c). This thermal tunability can be interpreted by tuning excitonic properties of MoS<sub>2</sub> via the environmental heating strategy. We first use the Lorentz oscillator model to fit the dielectric function of MoS<sub>2</sub> at room temperature<sup>[31]</sup>

$$\varepsilon = \varepsilon_b + \sum_{j=1}^3 f_j \frac{E_{ex,j}^2}{E_{ex,j}^2 - E^2 - i\gamma_{ex,j}E} \quad (5)$$

where  $E$  is the photon energy,  $\varepsilon_b$  is the background permittivity,  $f_j$ ,  $E_{ex,j}$ , and  $\gamma_{ex,j}$  are the oscillator strengths, exciton energies, and exciton linewidths of the three oscillators (A, B, and C excitons), respectively. As shown in Figure 4d, a reasonably good fitting can be obtained (see Table S1 for fitting parameters), which permits the modelling of temperature-dependent dielectric function caused by exciton tuning.

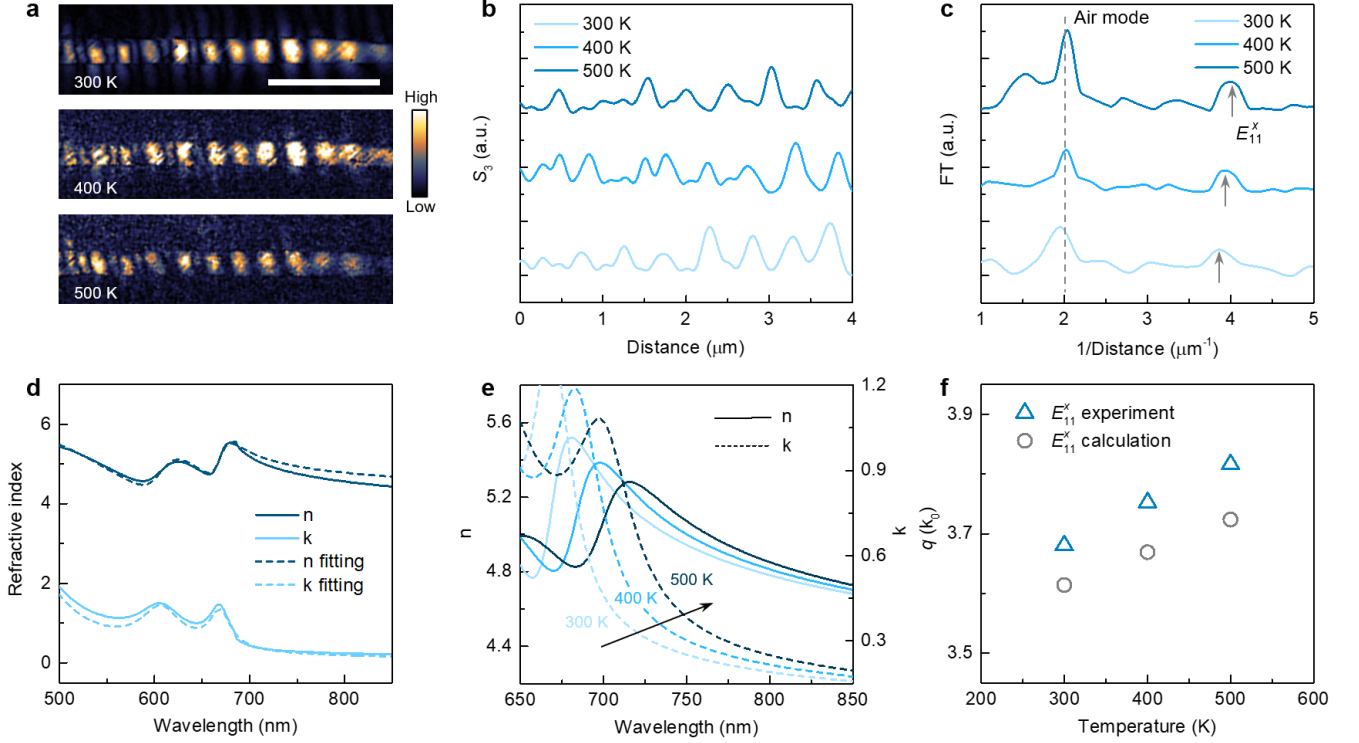


**Figure 4.** Thermal tunability of waveguide modes. a) Near-field images of a MoS<sub>2</sub> nanowire with a thickness of 80 nm under different temperatures and at the wavelength of 800 nm. b,c) The real-space fringe profiles and corresponding FT profiles. d) Dielectric function of bulk MoS<sub>2</sub> reported by Ref. <sup>[32]</sup> (solid curves) and its fitting (dashed curves) by the Lorentz oscillator model. e) The modelled temperature-dependent dielectric function of bulk MoS<sub>2</sub> after considering the exciton energy redshift and linewidth broadening at higher temperatures. f) Experimental and theoretical data of the  $E_{11}^x$  mode. Scale bar: (a) 2  $\mu\text{m}$ .

The temperature-dependent exciton energy and linewidth can be described by<sup>[33, 34]</sup>

$$E_{ex}(T) = E_{ex}(0) - S\langle\hbar\omega\rangle[\coth(\frac{\langle\hbar\omega\rangle}{2k_B T}) - 1] \quad (6)$$

$$\gamma_{ex}(T) = \gamma_{ex}(0) + \gamma'T \quad (7)$$

where  $T$  is the temperature,  $E_{ex}(T)$  and  $\gamma_{ex}(T)$  are the energy and linewidth of excitons at the temperature of  $T$ , respectively,  $E_{ex}(0)$  and  $\gamma_{ex}(0)$  are the energy and linewidth of excitons at 0 K, respectively,  $S$  is a dimensionless coupling constant to phonons,  $\langle \hbar\omega \rangle$  is the average phonon energy,  $k_B$  is the Boltzmann constant, and  $\gamma'$  is the exciton-phonon coupling strength. We model the dielectric function of MoS<sub>2</sub> at higher temperatures after accounting for the energy redshift and linewidth broadening (Figure 4e, see Table S1 for fitting parameters). The theoretical wavevectors of the  $E_{11}^x$  mode under different temperatures are calculated based on the modeled dielectric function, which is in good agreement with the wavevectors measured by the near-field experiments (Figure 4f). Such thermal modulation of excitons in TMDC nanowires and the resultant tunability in optical waveguide modes provide additional possibility for applications in tunable photonic devices.

In summary, we report the near-field nanoimaging of guided modes in colloidal TMDC waveguides. High-quality MoS<sub>2</sub> nanowires are prepared in a scalable way without the need of lithographic methods. In addition to the thickness and photon energy dispersion, we demonstrate the thermal tunability of the waveguide mode in TMDC nanowires through the exciton tuning strategy. This approach is expected to be applicable to other TMDC nanostructures as well. Our results show the potential of high-index TMDC materials for applications in integrated nanophotonics and tunable optical components. Moreover, being in the colloidal state, the TMDC nanowires reported here provide additional advantages for practical implementation, such as on-demand deposition to any substrates as well as easy integration with optical and electric manipulation techniques<sup>[23, 35-37]</sup> for controlled positioning and assembly of TMDC nanostructures with enhanced functionalities.

## Experimental Section

*Synthesis of colloidal TMDC waveguides.* MoO<sub>3</sub> nanowires are first synthesized as the precursor and template to prepare MoS<sub>2</sub> nanowires. In a typical hydrothermal synthesis, 1 g ammonium heptamolybdate tetrahydrate ((NH<sub>4</sub>)<sub>6</sub>Mo<sub>7</sub>O<sub>24</sub>·4H<sub>2</sub>O) is added into 20 mL deionized (DI) water, followed by vigorous stirring. After adding 5 mL HNO<sub>3</sub>, the solution is transferred to a 30 ml Teflon autoclave, which is maintained at 180 °C for 20 hours to obtain the powder of MoO<sub>3</sub> nanowires. Next, MoS<sub>2</sub> nanowires are prepared by a standard chemical vapor deposition method in a vacuum tube furnace. Two quartz boats filled with 0.5 g sulfur powder and 0.1 g MoO<sub>3</sub> nanowires, respectively, are placed into a one-end-sealed quartz tube with a separated distance of 20 cm. The tube pressure is reduced to 20 mTorr and Ar gas (50 sccm) is used as the carrier gas. The reaction temperature is set to 500 °C for 30 min to convert MoO<sub>3</sub>

nanowires into hybrid MoS<sub>2</sub>/MoO<sub>2</sub> nanowires. Last, a second heating cycle at 900 °C for 30 min is carried out to convert hybrid nanowires into pure MoS<sub>2</sub> nanowires.

*Materials characterizations.* The morphology of MoS<sub>2</sub> nanowires were characterized using a FEI Quanta 650 SEM and the Raman measurement was conducted with a Renishaw system using a 532 nm wavelength laser.

*Near-field nanoimaging.* The setup is developed based on a commercial near-field optical microscopy system (Molecular Vista).<sup>[38]</sup> A platinum-coated AFM tip with a tapping frequency  $\Omega$  of ~250 kHz and an apex radius of ~25 nm is used. A femtosecond laser beam from Spectra Physics with tunable wavelengths from 750 to 850 nm is directed to the AFM tip via a parabolic mirror. The typical optical intensity of the laser beam before entering the AFM chamber is ~ 0.5 mW. The scattered light is then collected by the parabolic mirror and redirected to an avalanche photodiode detector (Thorlabs) after it interferes with a reference beam from the reference mirror, per the scheme known as homodyne detection.<sup>[39]</sup> The signal from the detector is sent to a lock-in amplifier for signal demodulation at the third harmonic of the tapping frequency to suppress the background noise.

*Optical simulations.* The calculated in-plane wavevector (or propagation constant)  $q$  by the Marcatili method was confirmed by simulations using a commercial package (COMSOL Multiphysics 5.2, wave optics module) based on finite element method. A waveguide was modeled on its cross-sectional plane as a rectangle with rounded corners ( $r_c = 20$  nm), a fixed width ( $w = 300$  nm), and a varying thickness  $d$ , sitting on a semi-infinite substrate with an index  $n_s = 1.5$ . By using the mode analysis solver, possible effective mode indices were searched around the refractive index of MoS<sub>2</sub> at 800 nm wavelength.

## Supporting Information

Supporting Information is available from the Wiley Online Library or from the author.

## Acknowledgments

J.L. and R.Y. contributed equally to this work. We thank Dr. Guangwei Hu for helpful discussions. C.P.G. acknowledges the financial support from Laser Prismatic under the DOE SBIR Phase 2 grant DE-SC0018461. Y.Z. acknowledges the financial support of National Science Foundation (NSF-ECCS-2001650) and the National Institute of General Medical Sciences of the National Institutes of Health (R01GM146962). D. F. thanks the support from Welch Foundation (F-1734), National Science

Foundation (CMMI- 1563382 and EECS-1710922, EECS-1930649 in part). Part of this work by Y.R. was performed under the auspices of the U.S. Department of Energy by Lawrence Livermore National Laboratory under Contract DEAC52-07NA27344.

## References

- [1] Q. H. Wang, K. Kalantar-Zadeh, A. Kis, J. N. Coleman, M. S. Strano, *Nat. Nanotechnol.* **2012**, *7*, 699.
- [2] G. Wang, A. Chernikov, M. M. Glazov, T. F. Heinz, X. Marie, T. Amand, B. Urbaszek, *Rev. Mod. Phys.* **2018**, *90*, 021001.
- [3] S. Manzeli, D. Ovchinnikov, D. Pasquier, O. V. Yazyev, A. Kis, *Nat. Rev. Mater.* **2017**, *2*, 17033.
- [4] G. Hu, X. Hong, K. Wang, J. Wu, H.-X. Xu, W. Zhao, W. Liu, S. Zhang, F. Garcia-Vidal, B. Wang, P. Lu, C.-W. Qiu, *Nat. Photonics* **2019**, *13*, 467.
- [5] J. Pu, T. Takenobu, *Adv. Mater.* **2018**, *30*, 1707627.
- [6] D. Kufer, G. Konstantatos, *Nano Lett.* **2015**, *15*, 7307.
- [7] S. Jahani, Z. Jacob, *Nat. Nanotechnol.* **2016**, *11*, 23.
- [8] A. I. Kuznetsov, A. E. Miroshnichenko, M. L. Brongersma, Y. S. Kivshar, B. Luk'yanchuk, *Science* **2016**, *354*.
- [9] I. Staude, J. Schilling, *Nat. Photonics* **2017**, *11*, 274.
- [10] A. Arbabi, Y. Horie, M. Bagheri, A. Faraon, *Nat. Nanotechnol.* **2015**, *10*, 937.
- [11] S. Kruk, A. Poddubny, D. Smirnova, L. Wang, A. Slobozhanyuk, A. Shorokhov, I. Kravchenko, B. Luther-Davies, Y. Kivshar, *Nat. Nanotechnol.* **2019**, *14*, 126.
- [12] J. Li, M. Wang, Z. Wu, H. Li, G. Hu, T. Jiang, J. Guo, Y. Liu, K. Yao, Z. Chen, J. Fang, D. Fan, B. A. Korgel, A. Alu, Y. Zheng, *Nano Lett.* **2021**, *21*, 973.
- [13] R. Verre, D. G. Baranov, B. Munkhbat, J. Cuadra, M. Kall, T. Shegai, *Nat. Nanotechnol.* **2019**, *14*, 679.
- [14] T. D. Green, D. G. Baranov, B. Munkhbat, R. Verre, T. Shegai, M. Käll, *Optica* **2020**, *7*, 680.
- [15] G. I. Tselikov, G. A. Ermolaev, A. A. Popov, G. V. Tikhonowski, D. A. Panova, A. S. Taradin, A. A. Vyshnevyy, A. V. Syuy, S. M. Klimentov, S. M. Novikov, A. B. Evlyukhin, A. V. Kabashin, A. V. Arsenin, K. S. Novoselov, V. S. Volkov, *Proc. Natl. Acad. Sci. U. S. A.* **2022**, *119*, e2208830119.
- [16] B. Munkhbat, D. G. Baranov, M. Stührenberg, M. Wersäll, A. Bisht, T. Shegai, *ACS Photonics* **2019**, *6*, 139.
- [17] J. Li, K. Yao, Y. Huang, J. Fang, P. S. Kollipara, D. E. Fan, Y. Zheng, *Adv. Mater.* **2022**, *34*, e2200656.
- [18] C. T. Chen, J. Pedrini, E. A. Gaulding, C. Kastl, G. Calafiore, S. Dhuey, T. R. Kuykendall, S. Cabrini, F. M. Toma, S. Aloni, A. M. Schwartzberg, *Sci. Rep.* **2019**, *9*, 2768.
- [19] G. A. Ermolaev, D. V. Grudin, Y. V. Stebunov, K. V. Voronin, V. G. Kravets, J. Duan, A. B. Mazitov, G. I. Tselikov, A. Bylinkin, D. I. Yakubovsky, S. M. Novikov, D. G. Baranov, A. Y. Nikitin, I. A. Kruglov, T. Shegai, P. Alonso-González, A. N. Grigorenko, A. V. Arsenin, K. S. Novoselov, V. S. Volkov, *Nat. Commun.* **2021**, *12*, 854.
- [20] X. Han, K. Wang, X. Xing, M. Wang, P. Lu, *ACS Photonics* **2018**, *5*, 3970.
- [21] H. Ling, A. Manna, J. Shen, H.-T. Tung, D. Sharp, J. Fröch, S. Dai, A. Majumdar, A. R. Davoyan, *arXiv preprint arXiv:2302.06053* **2023**.
- [22] B. Munkhbat, B. Küçüköz, D. G. Baranov, T. J. Antosiewicz, T. O. Shegai, *Laser Photonics Rev.* **2023**, *17*, 2200057.
- [23] Y. Huang, K. Yu, H. Li, K. Xu, Z. Liang, D. Walker, P. Ferreira, P. Fischer, D. Fan, *Adv. Mater.* **2020**, *32*, 2003439.
- [24] L. Lin, J. Li, W. Li, M. N. Yogeesh, J. Shi, X. L. Peng, Y. Liu, B. B. Rajeeva, M. F. Becker, Y. Liu, D. Akinwande, Y. Zheng, *Adv. Funct. Mater.* **2018**, *28*, 1803990.
- [25] X. Chen, D. Hu, R. Mescall, G. You, D. N. Basov, Q. Dai, M. Liu, *Adv. Mater.* **2019**, *31*, 1804774.
- [26] S. Dai, Z. Fei, Q. Ma, A. S. Rodin, M. Wagner, A. S. McLeod, M. K. Liu, W. Gannett, W. Regan, K. Watanabe, T. Taniguchi, M. Thiemens, G. Dominguez, A. H. C. Neto, A. Zettl, F. Keilmann, P. Jarillo-Herrero, M. M. Fogler, D. N. Basov, *Science* **2014**, *343*, 1125.
- [27] F. Hu, Y. Luan, M. E. Scott, J. Yan, D. G. Mandrus, X. Xu, Z. Fei, *Nat. Photonics* **2017**, *11*, 356.
- [28] D. Hu, X. Yang, C. Li, R. Liu, Z. Yao, H. Hu, S. N. G. Corder, J. Chen, Z. Sun, M. Liu, Q. Dai, *Nat. Commun.* **2017**, *8*, 1471.

- [29] Z. Fei, M. E. Scott, D. J. Gosztola, J. J. Foley, J. Yan, D. G. Mandrus, H. Wen, P. Zhou, D. W. Zhang, Y. Sun, J. R. Guest, S. K. Gray, W. Bao, G. P. Wiederrecht, X. Xu, *Phys. Rev. B* **2016**, *94*, 081402.
- [30] D. Marcuse, *Theory of dielectric optical waveguides*, Elsevier, **2013**.
- [31] Y. Li, A. Chernikov, X. Zhang, A. Rigosi, H. M. Hill, A. M. van der Zande, D. A. Chenet, E.-M. Shih, J. Hone, T. F. Heinz, *Phys. Rev. B* **2014**, *90*, 205422.
- [32] B. Song, H. Gu, M. Fang, X. Chen, H. Jiang, R. Wang, T. Zhai, Y.-T. Ho, S. Liu, *Adv. Opt. Mater.* **2019**, *7*, 1801250.
- [33] K. P. O'Donnell, X. Chen, *Appl. Phys. Lett.* **1991**, *58*, 2924.
- [34] G. Moody, C. Kavir Dass, K. Hao, C.-H. Chen, L.-J. Li, A. Singh, K. Tran, G. Clark, X. Xu, G. Berghäuser, E. Malic, A. Knorr, X. Li, *Nat. Commun.* **2015**, *6*, 8315.
- [35] J. Li, Y. Liu, L. Lin, M. Wang, T. Jiang, J. Guo, H. Ding, P. S. Kollipara, Y. Inoue, D. Fan, B. A. Korgel, Y. Zheng, *Nat. Commun.* **2019**, *10*, 5672.
- [36] D. L. Fan, F. Q. Zhu, R. C. Cammarata, C. L. Chien, *Nano Today* **2011**, *6*, 339.
- [37] J. Li, E. H. Hill, L. Lin, Y. Zheng, *ACS Nano* **2019**, *13*, 3783.
- [38] J. Li, R. Yang, Y. Rho, P. Ci, M. Eliceiri, H. K. Park, J. Wu, C. P. Grigoropoulos, *Nano Lett.* **2023**, *23*, 1445.
- [39] M. Mrejen, L. Yadgarov, A. Levanon, H. Suchowski, *Sci. Adv.* **2019**, *5*, eaat9618.